Supplementary Materials:

Precisely Segmented PEEK-Ionene + Ionic Liquid Composite Membranes for CO_2 Separation

Sudhir Ravula,[a] Ying Chen,[b] Kevin W. Wise,[a] Pravin S. Shinde,[a] Eric D. Walter,[c] Abhi Karkamkar,[c] David J. Heldebrant[d,e] and Jason E. Bara[a,*]

[a] **Department of Chemical & Biological Engineering, University of Alabama, Tuscaloosa, AL 35487-0203 USA**
[b] **Physical and Computational Sciences Directorate, Pacific Northwest National Laboratory, Richland, WA 99352 USA**
[c] **Environmental Molecular Sciences Laboratory, Pacific Northwest National Laboratory, Richland, WA 99352 USA**
[d] **Energy and Environment Directorate, Pacific Northwest National Laboratory, Richland, WA 99352 USA**
[e] **Department of Chemical Engineering and Bioengineering, Washington State University, Pullman, WA 99163 USA**

* Correspondence: jbara@eng.ua.edu

Received:; Published: date

Included are relevant supporting data referenced in the manuscript: “Precisely Segmented PEEK-ionene + Ionic Liquid Composite Membranes for CO_2 separation”. Structures, NMR, results are shown in the following sections.

The ^{1}H-NMR spectra for the monomers are outlined in the manuscript are included below, with corresponding structures included. Assignments and specific *ppm* assignments and splitting patterns are outlined in the manuscript.

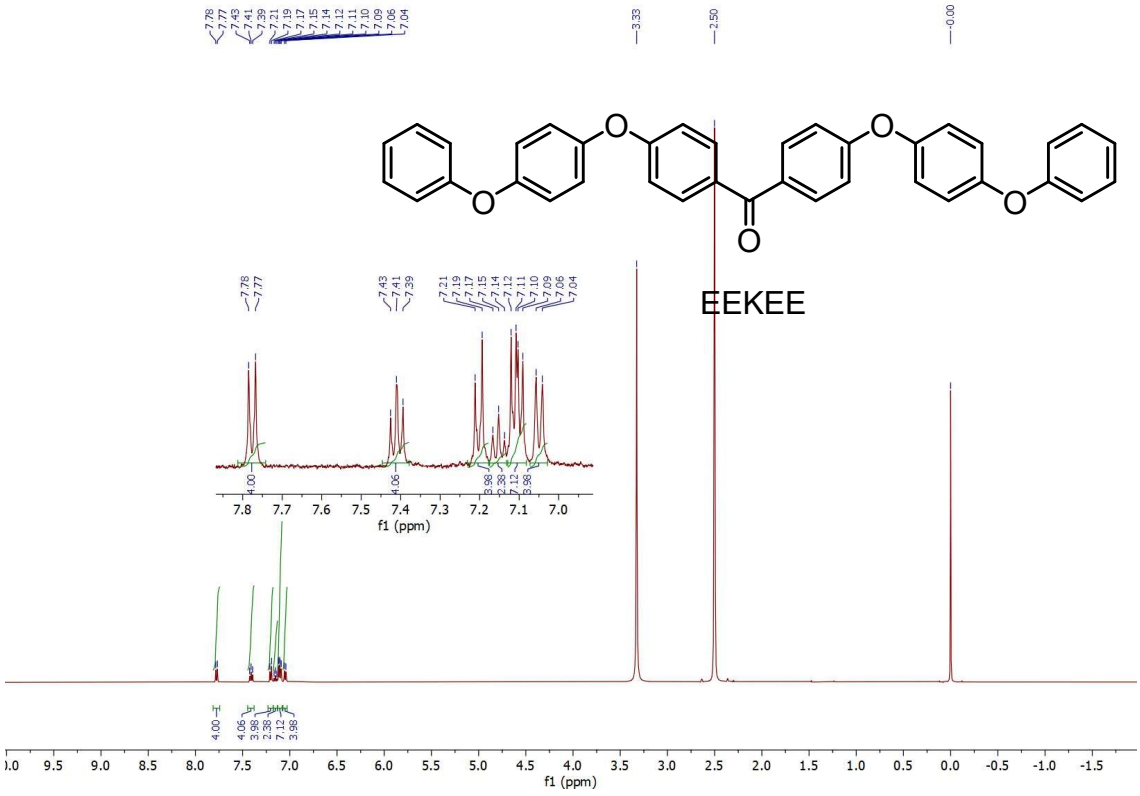

Figure S1. ^{1}H-NMR spectrum for EEKEE

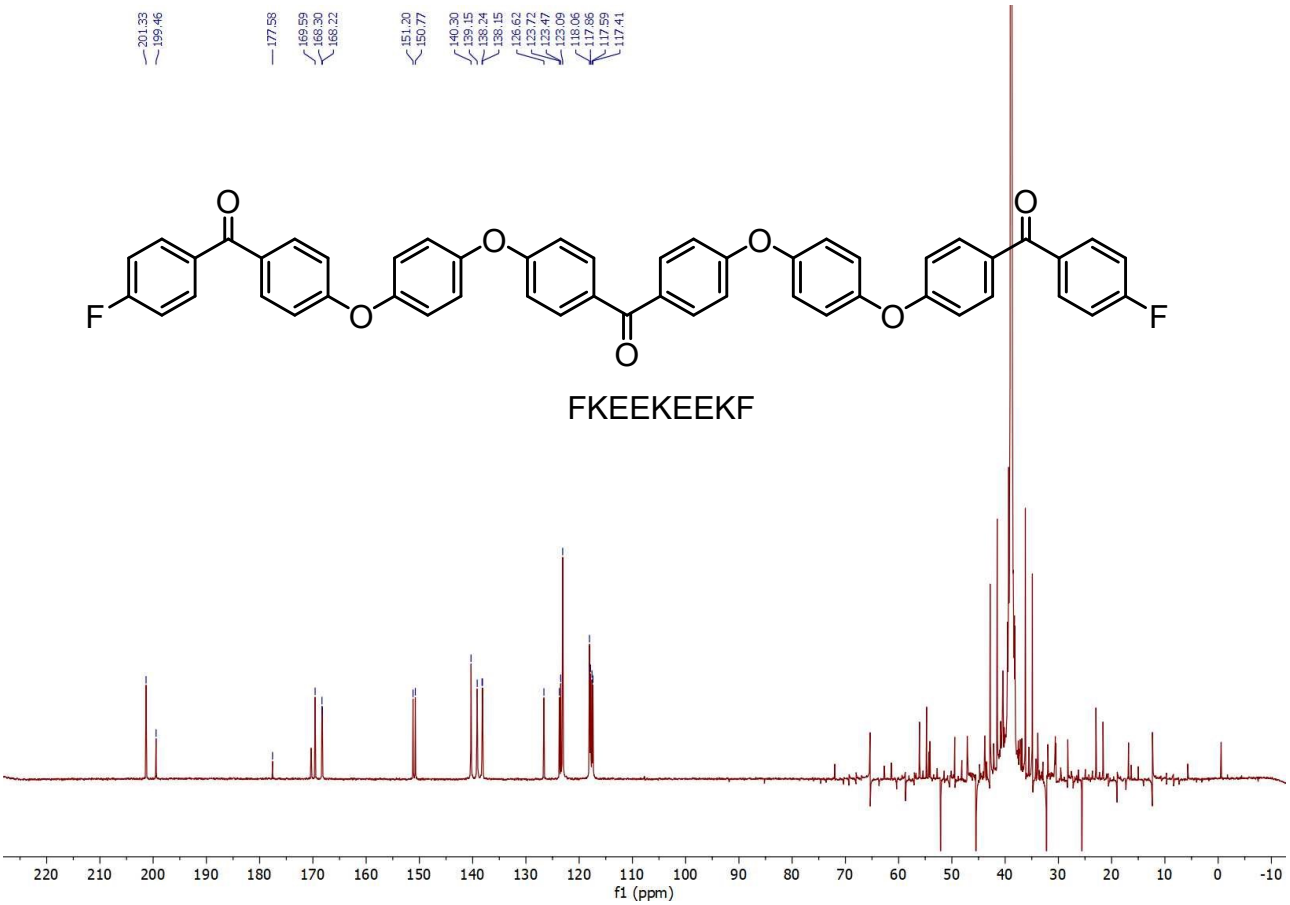

Figure S2. ^{13}C-NMR spectrum of FK(EEK)$_2$F. The spectrum was recorded in methanesulfonic acid and the signal in upward filed are due to the acid.

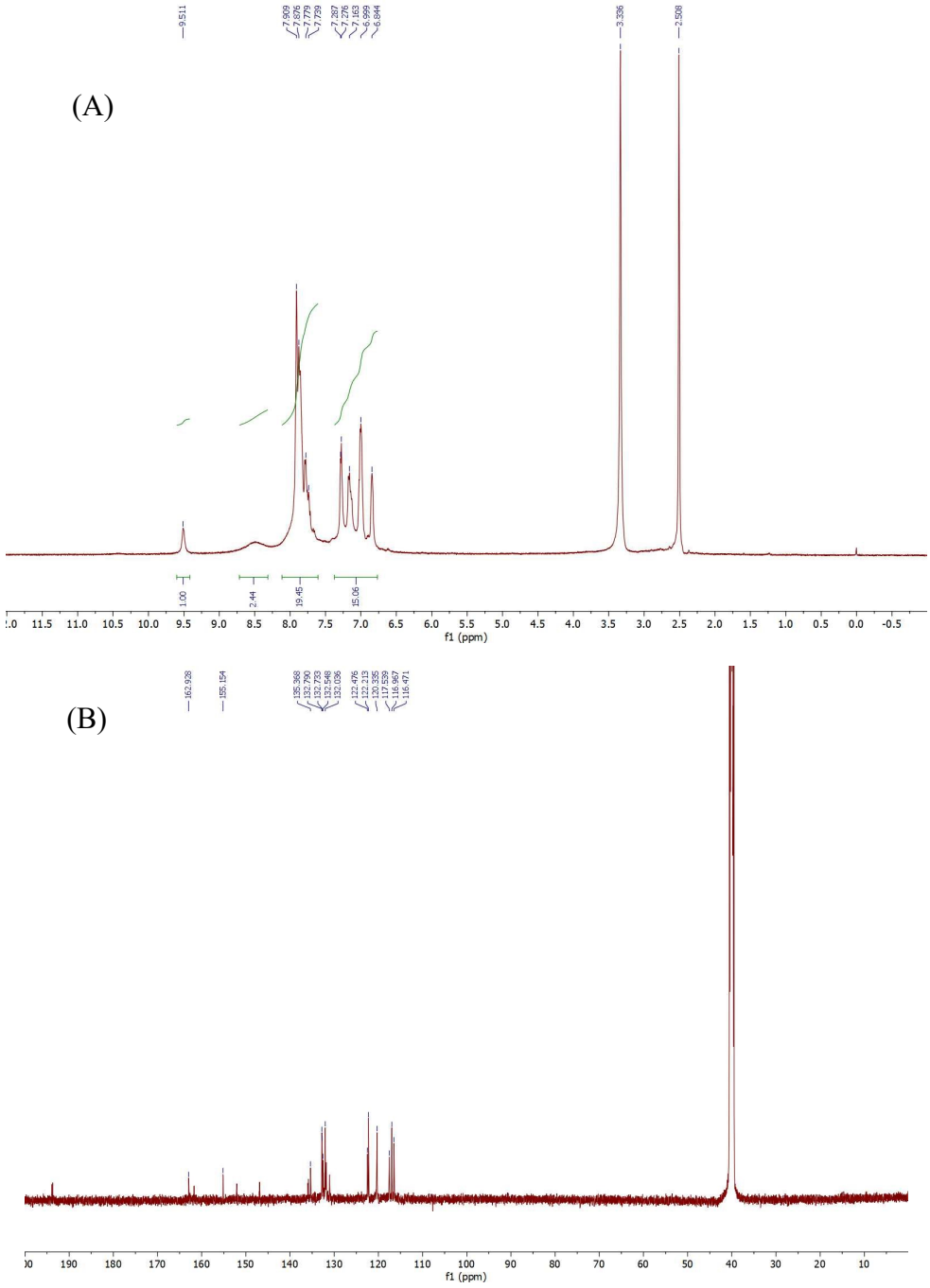

Figure S3. ^{1}H-NMR (A) and ^{13}C-NMR (B) spectrum of ImK(EEK)$_2$Im. The ImK(EEK)$_2$Im monomer is sparingly soluble at room temperature.

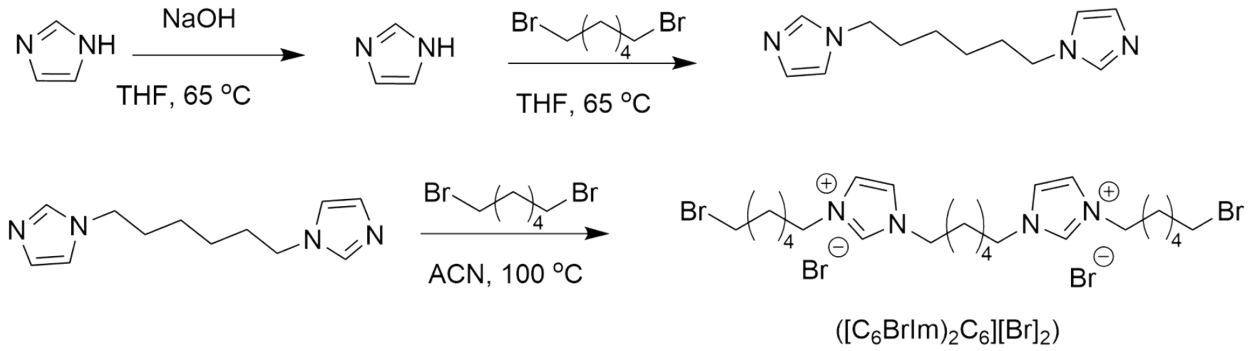

Figure S4. Schematic overview of aliphatic comonomer ($([C_6BrIm)_2C_6][Br]_2$)

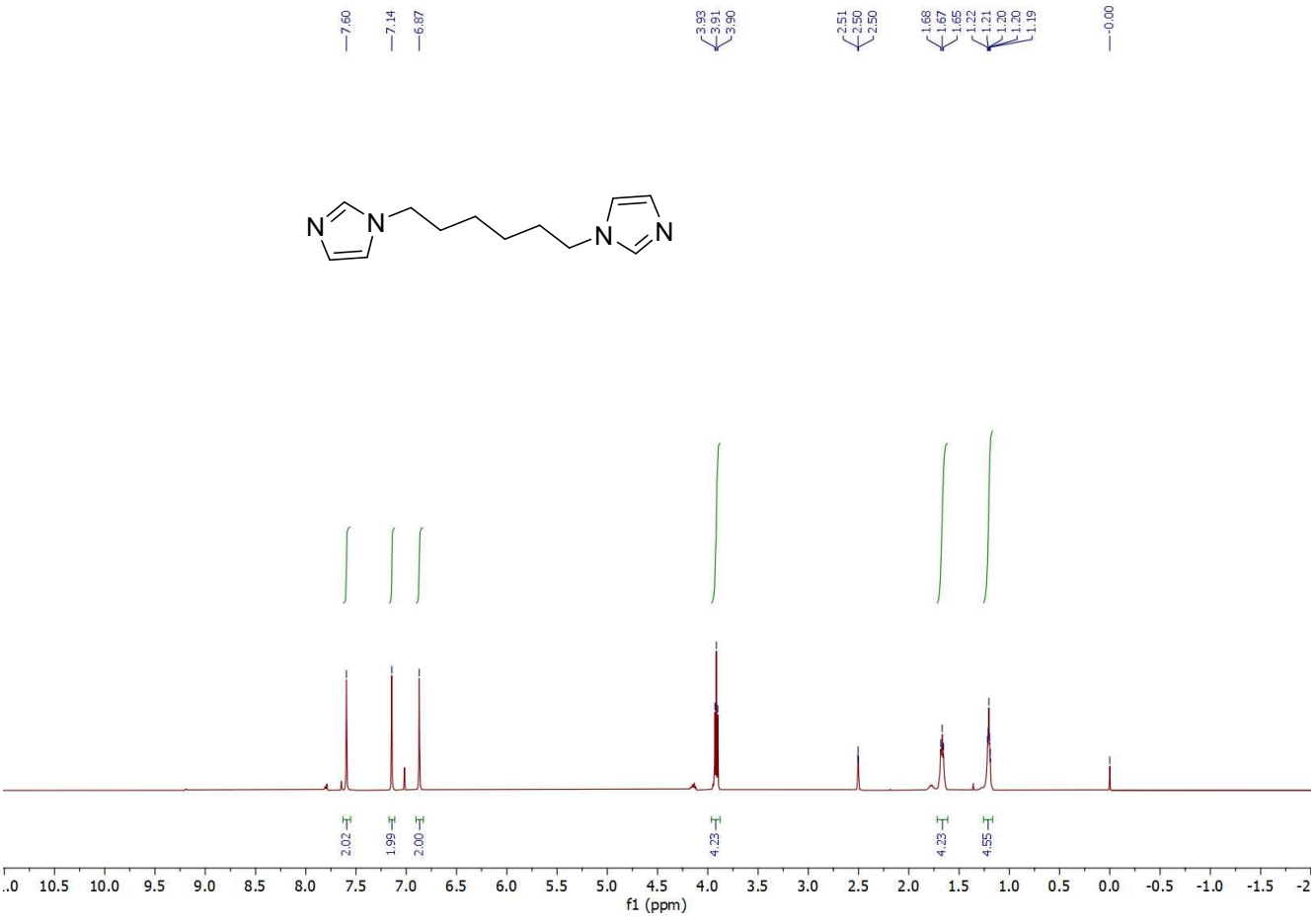

Figure S5. ^{1}H-NMR spectra of 1,6-bis(imidazole) hexane.

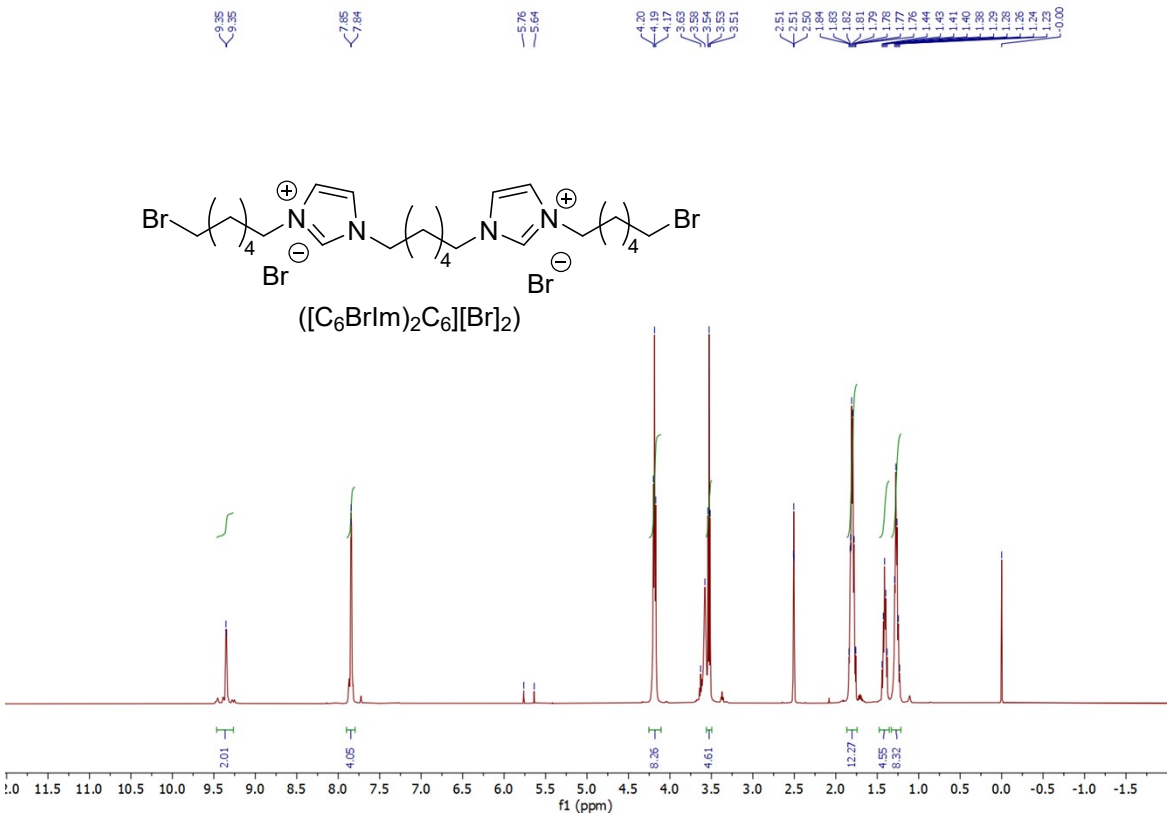

Figure S6. ^{1}H-NMR spectrum for comonomer [([C_6BrIm)$_2$Im][Br]$_2$

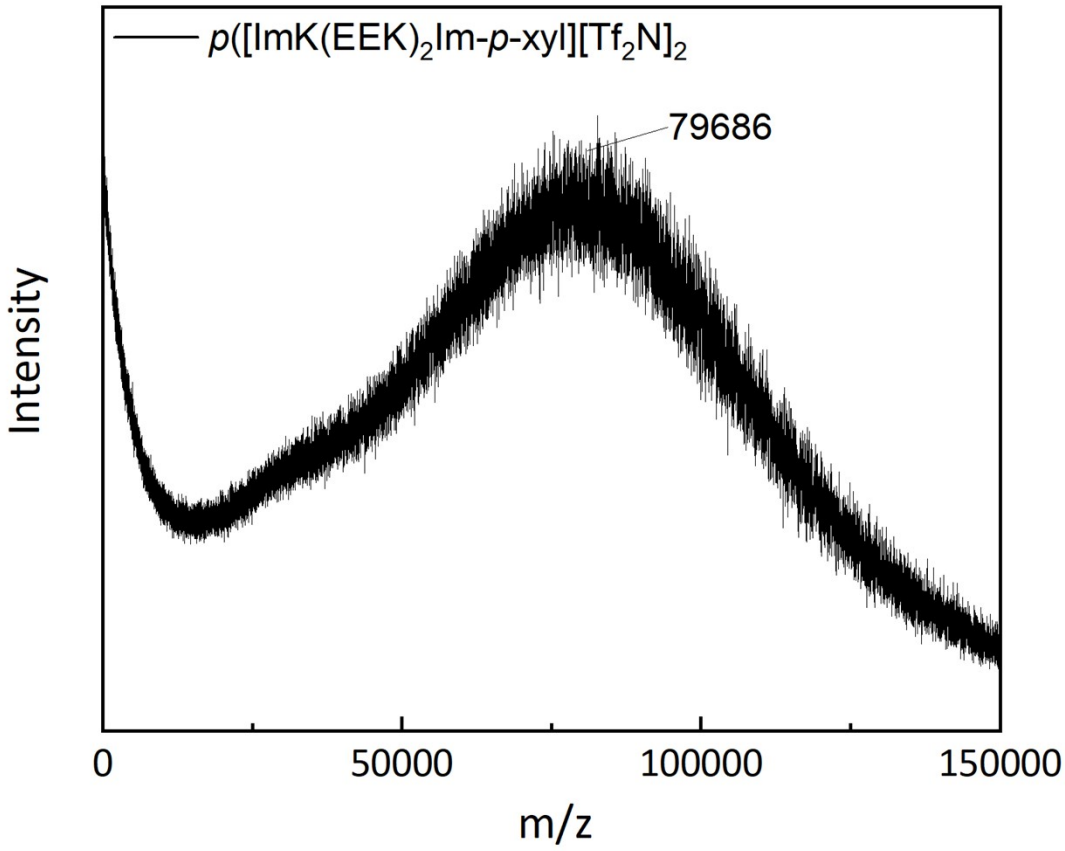

Figure S7: MALDI-TOF spectra for *p*([ImK(EEK)$_2$Im-*p*-xyl][Tf$_2$N]$_2$) (P1) ionene.

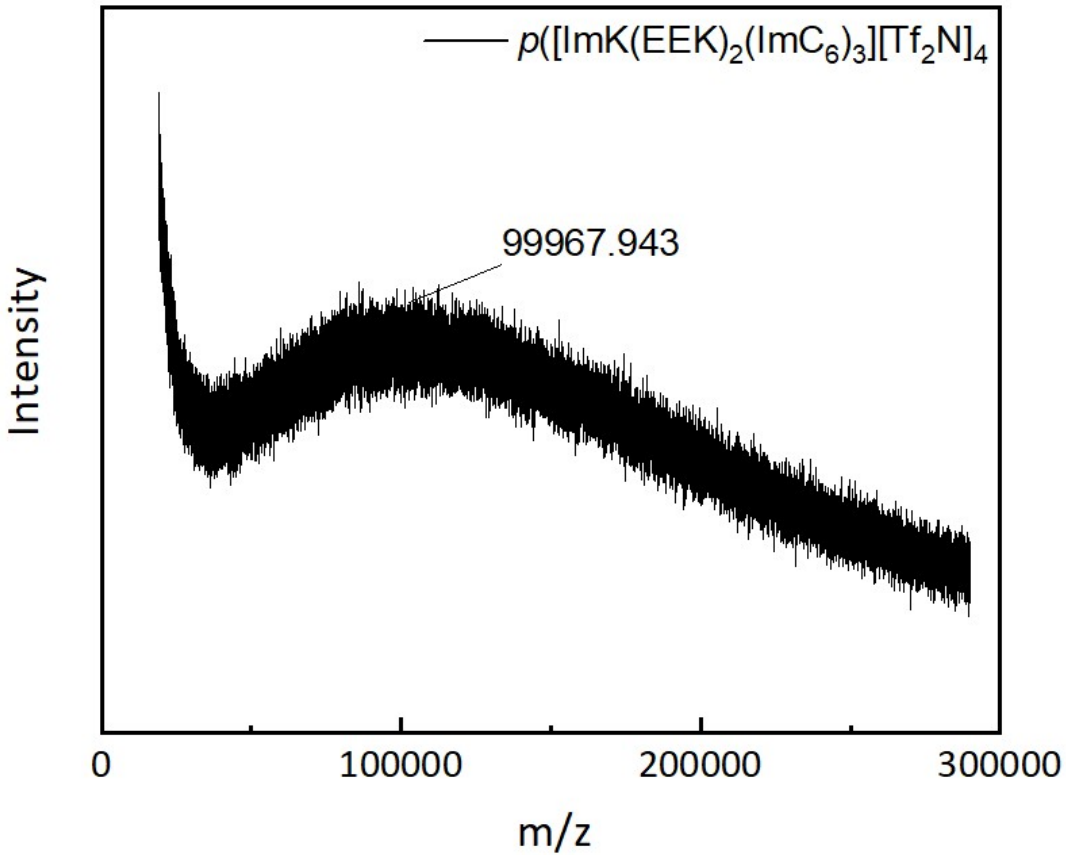

Figure S8: MALDI-TOF spectra for *p*([ImK(EEK)$_2$(ImC$_6$)$_3$][Tf$_2$N]$_4$) (P2) ionene.

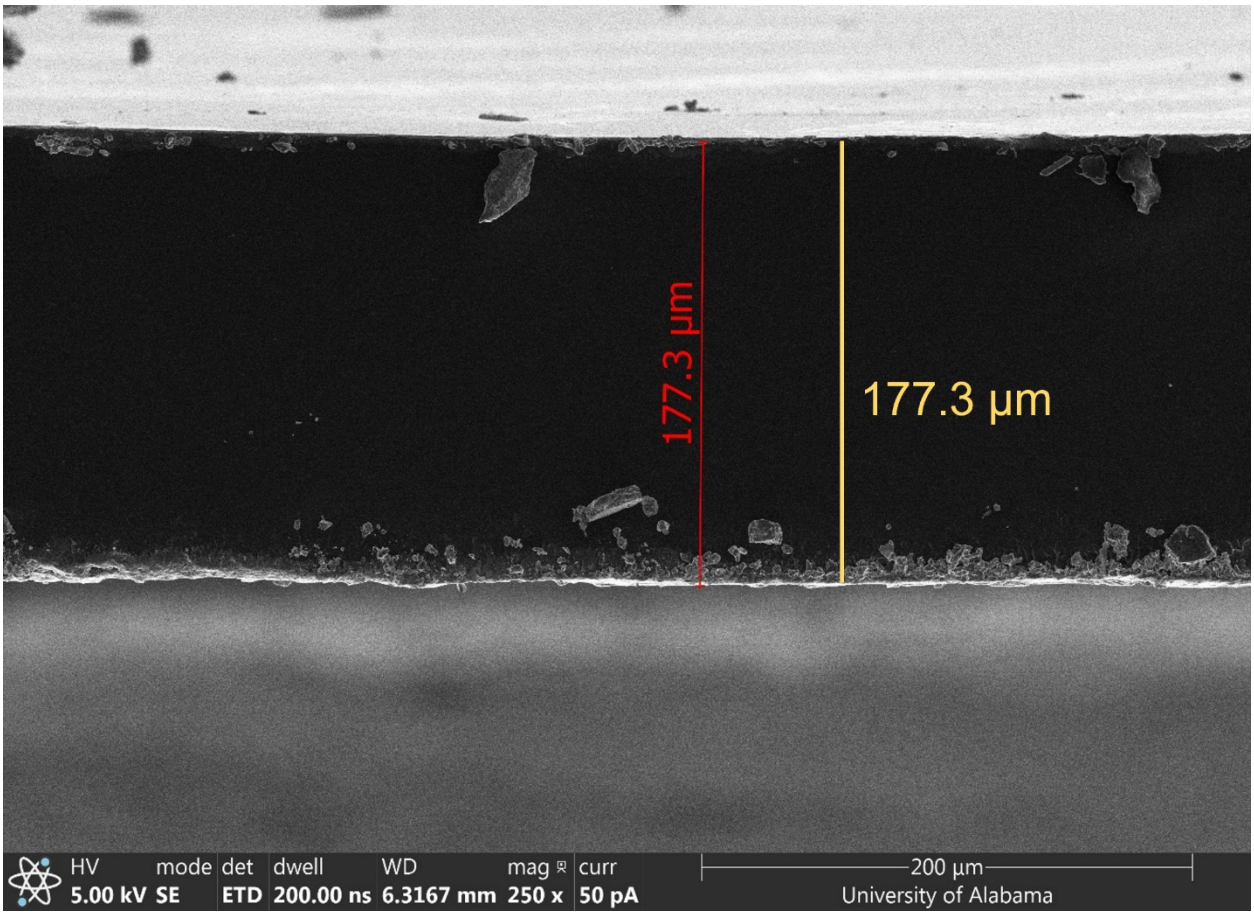

Figure S9: Cross-sectional scanning electron microscopy (SEM) image of *p*([ImK(EEK)$_2$Im-*p*-xyl][Tf$_2$N]$_2$) + 1 eq IL (P1 + 1 eq. IL). The cross-section was captured at 250X magnification.

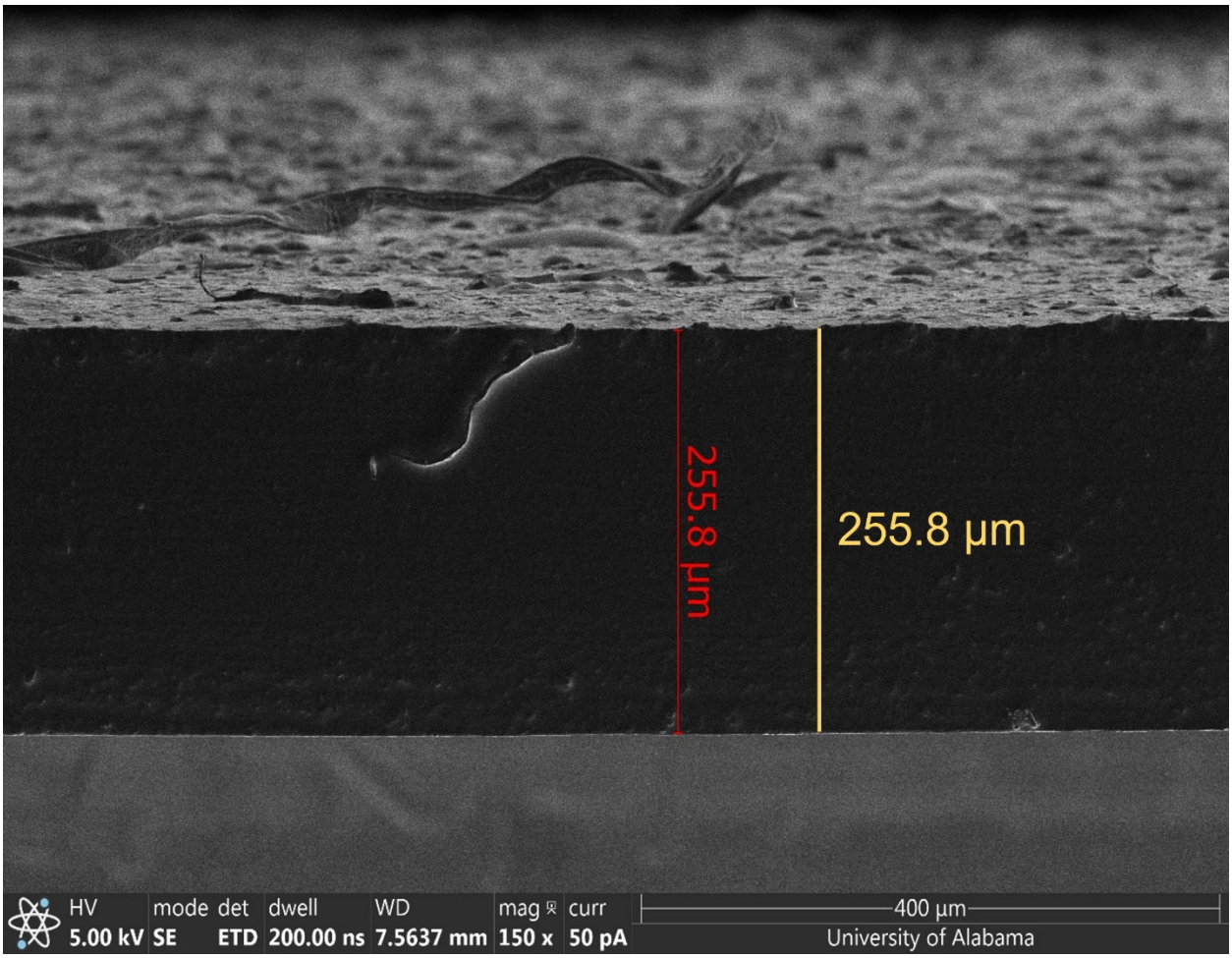

Figure S10: Cross-sectional scanning electron microscopy (SEM) image of *p*([ImK(EEK)$_2$Im-*p*-xyl][Tf$_2$N]$_2$) + 2 eq IL (P1 + 2 eq. IL). The cross-section was captured at 150X magnification.

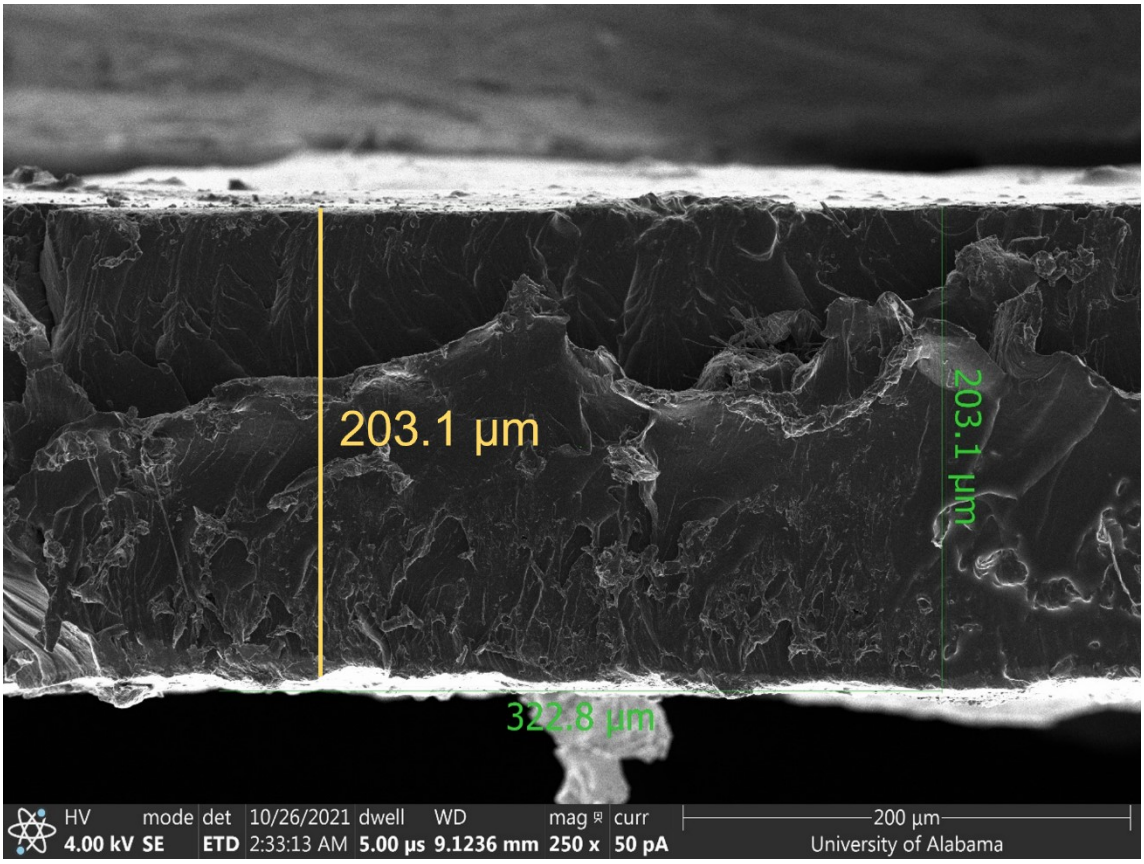

Figure S11: Cross-sectional scanning electron microscopy (SEM) image of *p*([ImK(EEK)$_2$(ImC$_6$)$_3$][Tf$_2$N]$_4$) + 1 eq IL (P2 + 1 eq. IL). The cross-section was captured at 250X magnification.

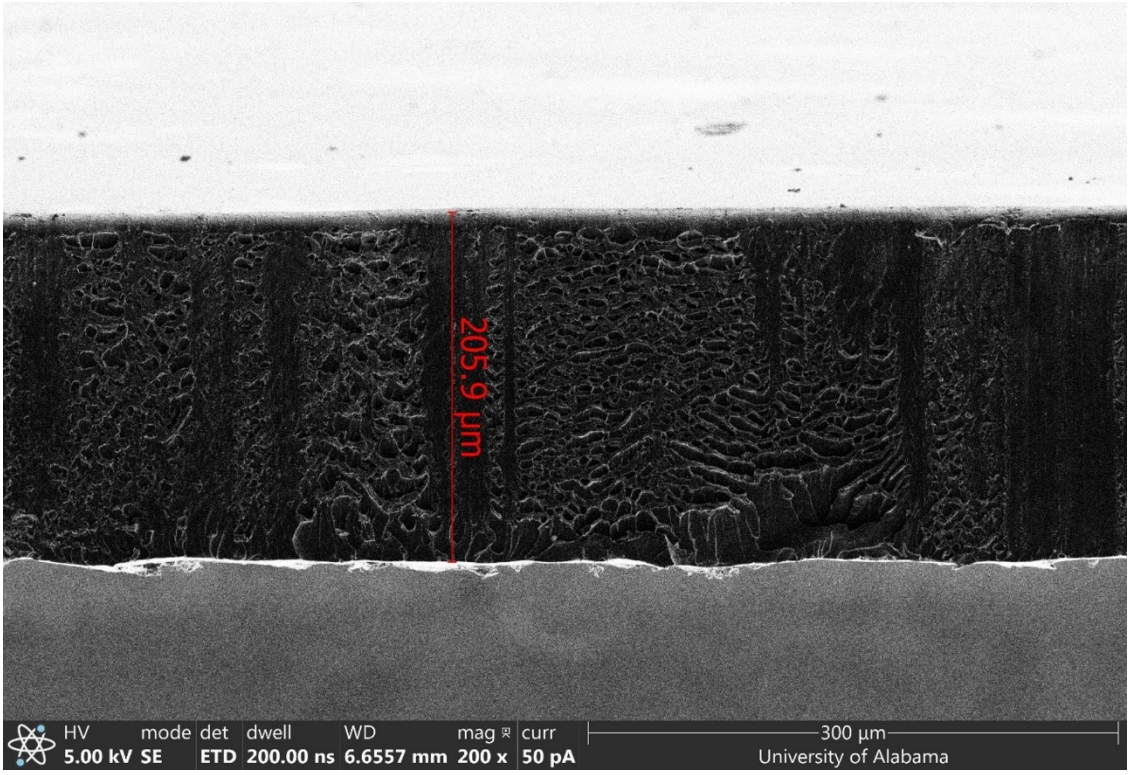

Figure S12: Cross-sectional scanning electron microscopy (SEM) image of *p*([ImK(EEK)$_2$(ImC_6)$_3$][Tf_2N]$_4$) + 2 eq IL (P2 + 2 eq. IL). The cross-section was captured at 200X magnification.

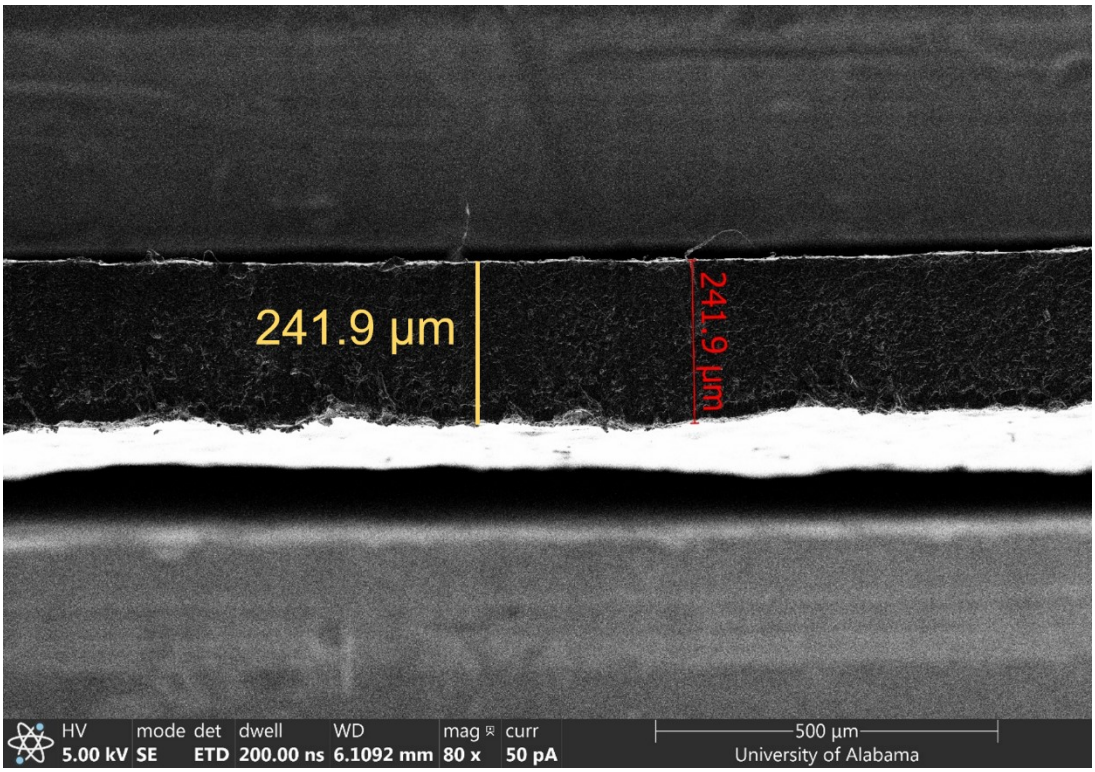

Figure S13: Cross-sectional scanning electron microscopy (SEM) image of *p*([ImK(EEK)$_2$(ImC$_6$)$_3$][Tf$_2$N]$_4$) + 3 eq IL (P2 + 3 eq. IL). The cross-section was captured at 80X magnification.

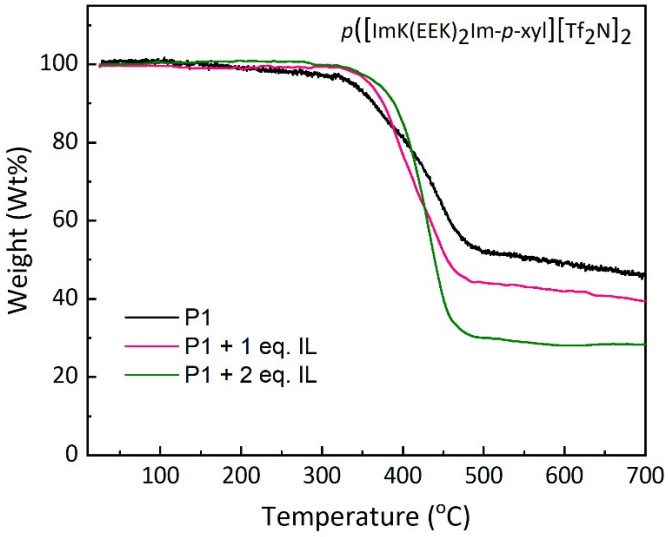

Figure S14: TGA data for *p*([ImK(EEK)$_2$Im-*p*-xyl][Tf_2N]$_2$) (P1) ionene and corresponding composites.

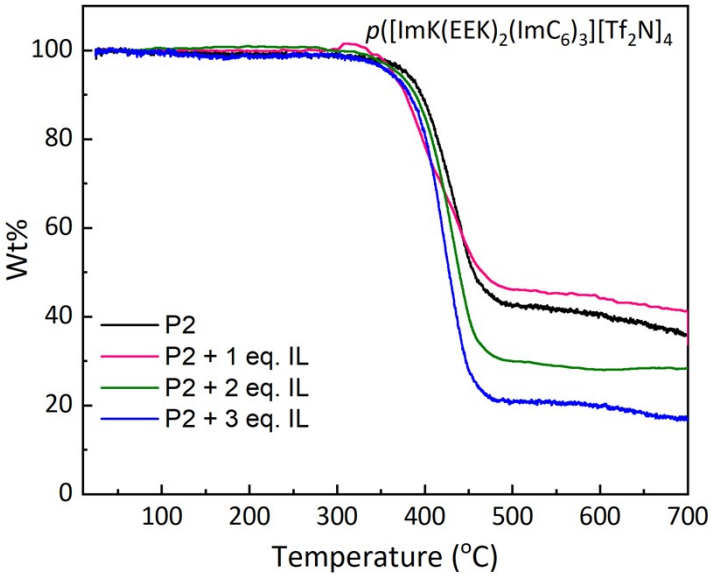

Figure S15: TGA data for *p*([ImK(EEK)$_2$(ImC_6)$_3$][Tf_2N]$_4$) (P2) ionene and corresponding composites.

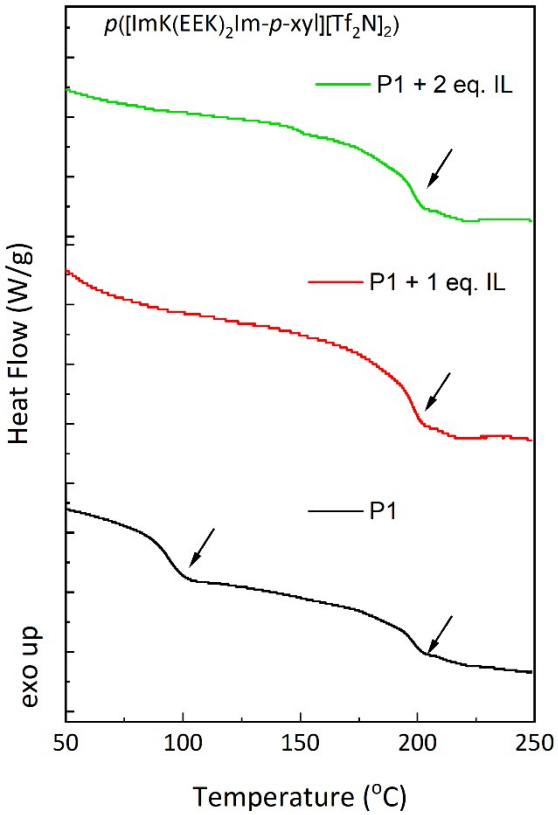

Figure S16: DSC scans for *p*([ImK(EEK)$_2$Im-*p*-xyl][Tf$_2$N]$_2$) (P1) ionene and corresponding composites. The transition observed around 198 °C is due to the aluminum pan used in this measurement.

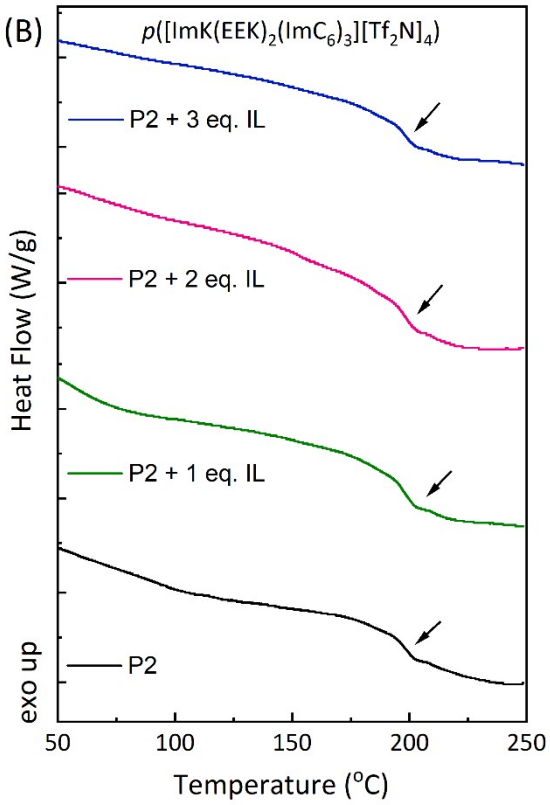

Figure S17: DSC scans for *p*([ImK(EEK)$_2$(ImC$_6$)$_3$][Tf$_2$N]$_4$) (P2) ionene and corresponding composites. The transition observed around 198 °C is due to the aluminum pan used in this measurement.

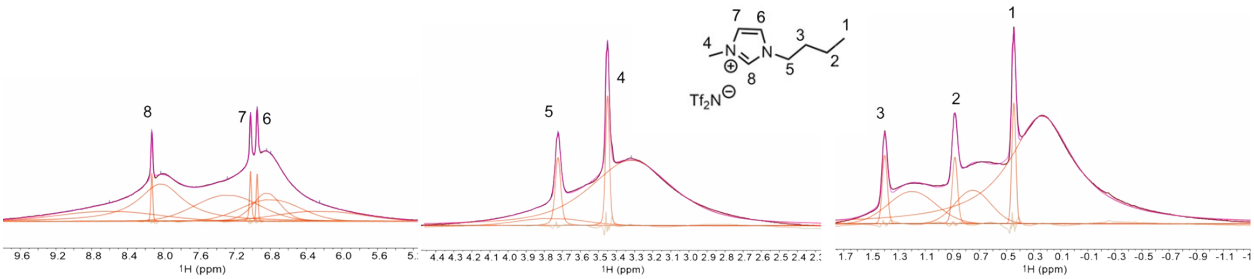

Figure S18. Spectral deconvolution of ^{1}H NMR reveals two local environments for incorporated IL.

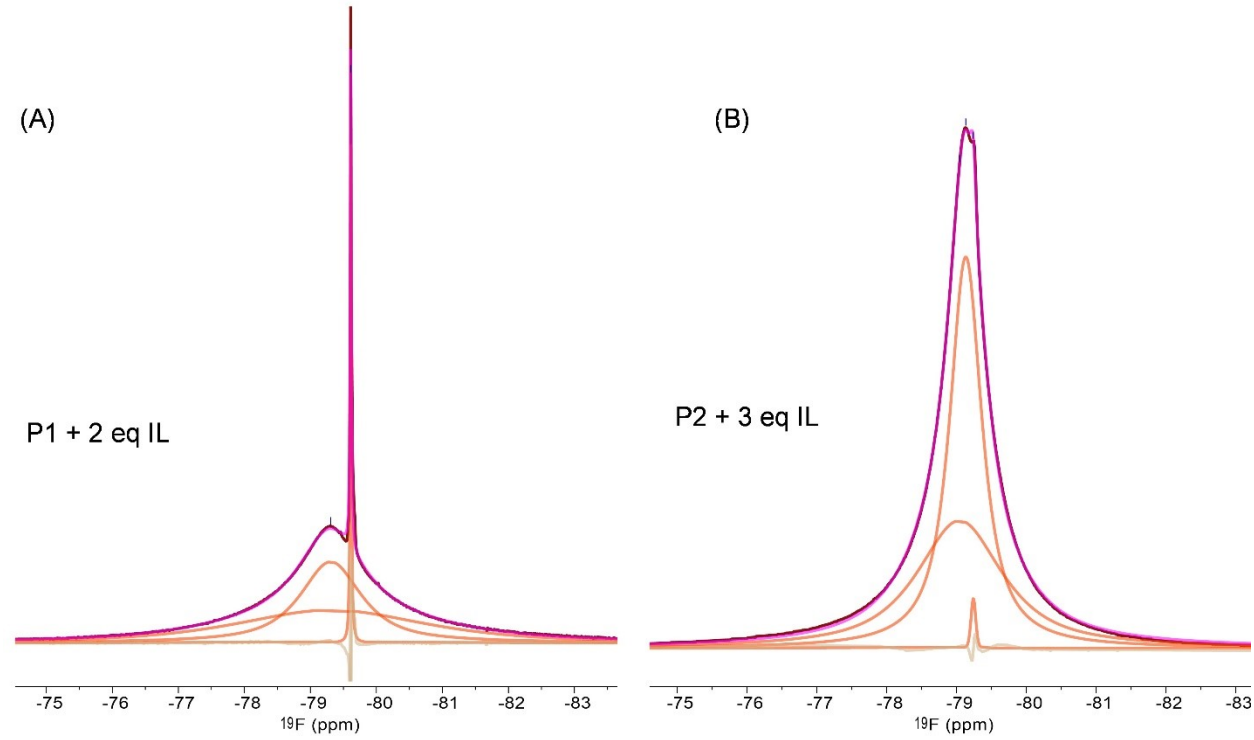

Figure S19. Spectral deconvolution of ^{19}H NMR spectra reveals three distinct components for Tf_2N^-.

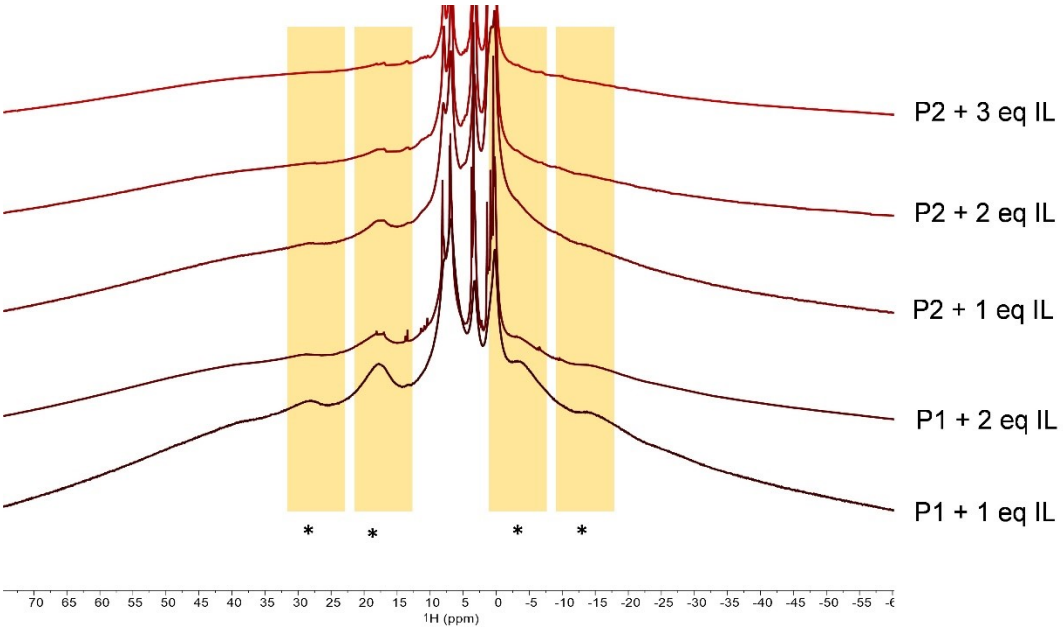

Figure S20. Solid-state ^{1}H MAS NMR spectra of PEEK-ionene polymers at a spinning speed of 6 kHz, with a wide spectral width to show all the spinning sides (labeled as asterisks).

Table S1. Pure gas diffusivity coefficient and solubility coefficient of PEEK ionene-IL composites

Membrane	Diffusivity[a] (D_{CO2})	Solubility[b] (S_{CO2})
P1 + 1 eq. IL	1.69 ± 0.21	2.31 ± 0.26
P1 + 2 eq. IL	5.73 ± 0.19	2.78 ± 0.10
P2 + 1 eq. IL	1.06 ± 0.10	1.98 ± 0.15
P2 + 2 eq. IL	3.70 ± 0.30	3.04 ± 0.25
P2 + 3 eq. IL	45.65 ± 0.15	1.70 ± 0.25

[a]Diffusivity coefficient (10^{-8} cm^2/s). [b]Solubility coefficient (10^{-2} $cmSTP^3$ cm^{-3} $cmHg^{-1}$) measured at 20 °C and 2 atm of feed pressure.

Note: The diffusivity and solubility of other gas molecules (O_2, N_2, and CH_4) have low coefficient values when compared to smaller gas molecules (CO_2). As the diffusivity measures how quickly a gas molecule can diffuse through a medium. It is influenced by several factors, including the size and shape of the cavities of the membrane, the mass of the diffusing gas molecule, temperature, and the pressure of the system. Since the pressure and area of the membrane used in this study are small, the rate of mass transfer per unit area for larger gas molecules are extremely lower compared to CO_2 gas molecules. When analyzing the diffusion rates, we observed that larger gas molecules were 3-5 × smaller than the CO_2 gas molecules. On the other hand, the solubility of other gas molecules are much lower as compared to CO_2, due to weaker interactions with the ILs. Therefore, the apolar molecules have negligible effect on the solubility coefficient with the IL loading capacity.

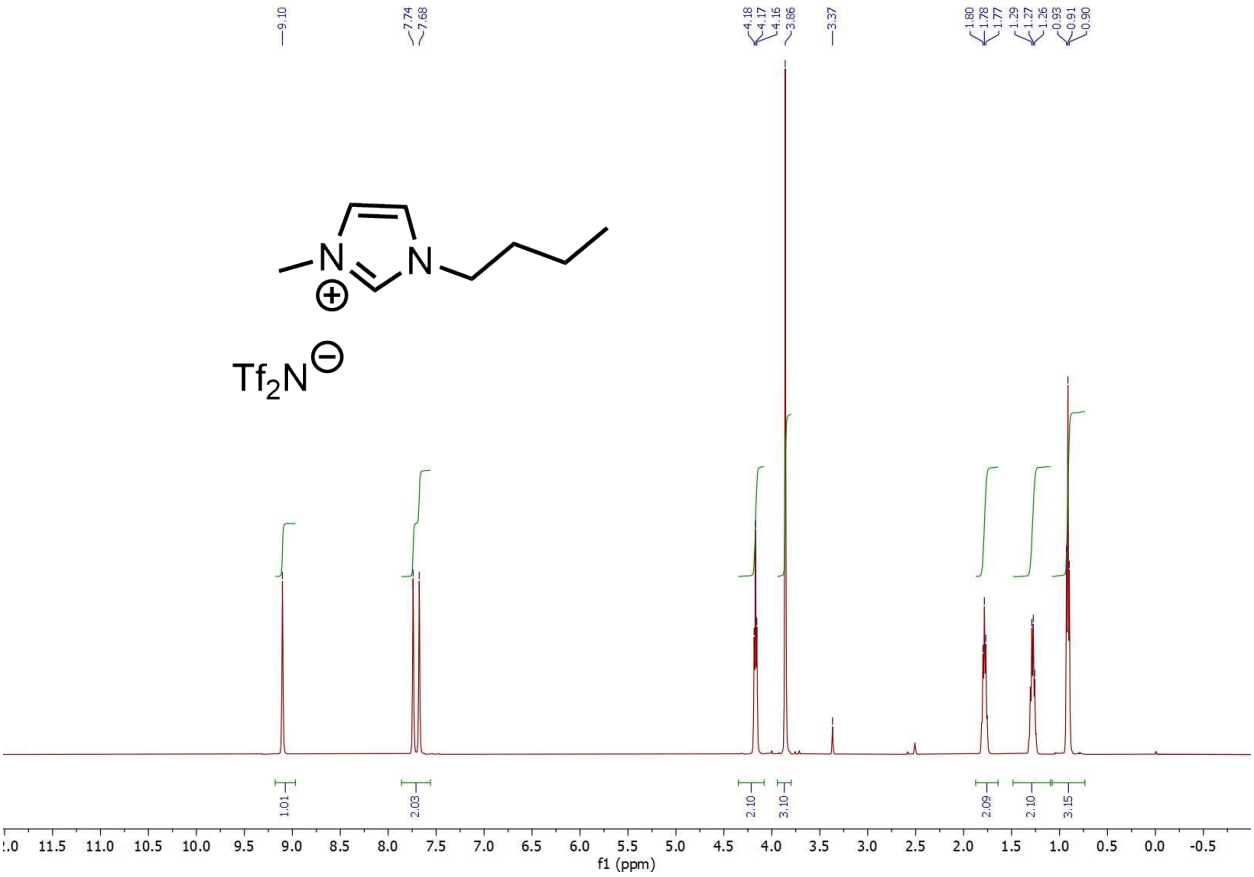

Figure S21: ^{1}H NMR of $[C_4mIm][Tf_2N]$ IL used in this study.